Thermocapillary instability of core-annular flows

Hsien-Hung Wei
Department of Chemical Engineering, National Cheng Kung University, Tainan 701, Taiwan

(Received 27 September 2004; accepted 25 August 2005; published online 13 October 2005)

Thermocapillary instability of a core-annular flow is asymptotically examined in the thin annulus limit. Two sets of scalings are established to study the interplays between base flows, interfacial tension, and thermocapillary effects. For each scaling case, an interfacial evolution equation is derived for describing the leading order stability of the system. Both linear and weakly nonlinear stabilities are examined. When the core fluid is warmer (cooler) than the wall, thermocapillarity linearly stabilizes (destabilizes) the system, and hence suppresses (promotes) the capillary instability. For a moderate thermocapillary force and a strong capillary force, the linear instability can be arrested within the weakly nonlinear regime. For a weak thermocapillary force and a moderately strong interfacial tension, the weakly nonlinear evolution is governed by a modified Kuramoto-Sivashinsky equation. The influence of thermocapillarity on the route to chaos is discussed. © *2005 American Institute of Physics*. [DOI: 10.1063/1.2085190]

I. INTRODUCTION

A two-fluid core-annular flow (CAF) consists of two immiscible fluids flowing concurrently in a tube, where one (annular) fluid wets the tube wall and surrounds the other (core) fluid. This flow system is often served as a useful model for a variety of processes such as lubricated pipelining,[1] packed beds,[2] enhanced oil recovery,[3] and liquid lining flows in airways.[4] The present study is in particular motivated from efforts to construct an appropriate model for understanding processes occurring in oil recovery. To recover oil that is lodged within capillary pores of rocks, one can displace oil with another immiscible fluid (usually water). This fluid-fluid displacement creates a train of slugs that travel through pores. An interfacial instability plays a decisive role in determining the efficiency of the recovery process. A growing interface due to capillary instability can cause the wetting layer to snap and bring the nonwetting phase in contact with the pore wall. This can retard the mobility of a slug, thereby hindering the recovery process.

The efficiency of recovery can be improved by adding surface-active agents that lower the surface tension, or by applying a hot gas stream that reduces the viscosity of crude oil. In either treatment, the temperature of the displacing fluid could be different from rocks that may be located in a scorching underground environment. This could induce thermal effects such as buoyancy and thermocapillarity, which might significantly influence the stability of the system and hence the efficiency of recovery. In an *ab initio* attempt to understand these effects on CAFs, we seek to investigate the role of thermocapillarity in affecting the stability thereof.

For *isothermal* CAFs, the dominant effects on the stability are capillarity and viscosity stratification. Capillarity destabilizes (stabilizes) the system when wavelengths of disturbances are longer (shorter) than the undisturbed interfacial circumference. Preziosi *et al.*[1] numerically solved the full Orr-Sommerfeld equations for examining the linear stability relevant to lubricated pipelines. They showed that for a more viscous core with a sufficiently large Reynolds number, viscosity stratification can overcome the long wave destabilization of capillarity and stabilize disturbances of all wavelengths. Georgiou *et al.*[5] developed an asymptotic theory to examine the linear stability of a vertical CAF in the thin-annulus limit. They showed that for a more viscous core, viscosity stratification could have a stabilizing effect in a range of the Reynolds number. For a more viscous annulus, however, viscosity stratification is destabilizing.

Frenkel *et al.*[6] and Papageorgiou *et al.*[7] derived Kuramoto-Sivashinsky equations for the weakly nonlinear interfacial dynamics of CAFs. The latter included the effects of core dynamics via viscosity stratification. These studies demonstrated that capillary instability can be arrested by nonlinear effects. Kerchman[8] studied the strongly nonlinear stability of CAFs and showed that the dynamics of the interface strongly depends on the capillary number, Ca, the ratio of viscous to interfacial tension forces based on the properties of the core fluid. A CAF configuration could either remain intact due to the nonlinear saturation of the capillary instability, or collapse due to the interface's bulging into the core. Recently, Kouris and Tsamopoulos[9,10] numerically solved the full Navier-Stokes equations of CAF and confirmed the dynamics revealed in early CAF studies.[7,8] As such, the stability of *isothermal* CAFs is fairly well understood.

As for nonisothermal systems, we focus on thermocapillary effects, i.e., temperature-induced interfacial tension gradient forces that drive fluids toward the higher-tension (lower-temperature) regions. Some previous studies on planar systems have revealed some features of instability arising from thermocapillarity. Pearson[11] first investigated the thermocapillary problem of a nondeformable fluid layer over a heated wall in the absence of gravity. Scriven and Sternling[12] extended the analysis by accounting for the effects of interfacial deformation. These studies indicated that thermocapillarity destabilizes the systems with heated walls. Goussis and Kelly[13] examined the instability of a liquid film flowing

down an inclined heated wall. They pointed out that there are two distinct mechanisms responsible for the thermocapillary destabilization. One mechanism is associated with interactions between the basic temperature profile and the disturbed velocity field.[14] The other mechanism arises from the modulation of the basic temperature at the deformed interface.[14,15]

Since planar interfacial flow systems inherently lack the circumferential component of the interfacial curvature, their stability features differ from those of cylindrical systems such as CAFs. Nevertheless, under some circumstances, the instability occurring in a planar system could be analogous to that in a CAF.[15] An example is the Rayleigh-Taylor instability that occurs when a heavier fluid is placed on top of another immiscible, lighter layer. Similar to the role of the circumferential capillarity in a CAF, destabilizing effects are induced by buoyancy forces arising from the density difference of the fluids. An interfacial tension force, accompanied only with the longitudinal curvature of the interface, is stabilizing. If there were a temperature gradient across the channel, the induced thermocapillary forces can either encourage or discourage the buoyancy-driven instability, depending on whether the plate is heated or cooled from the bottom.[15]

There are a few studies addressing how thermocapillarity affects the stability of interfacial flow in cylindrical systems. Dijkstra and Steen[16] studied the linear stability of a thermocapillary-driven flow on the exterior surface of the cylinder. They showed that complete stabilization could occur under certain conditions. Davalos-Orozco and You[17] studied the three-dimensional instability of a liquid layer flowing down a heated vertical cylinder. They examined both flows inside and outside the cylinder. Their study showed that thermocapillarity could excite instability due to azimuthal modes. The growth rate of an azimuthal mode could be faster than that of the axisymmetric mode in some range of parameters. This is in contrast with the isothermal flow where the axisymmetric mode is always the most unstable. However, as the Crispation number $\mathrm{Cr}=\mathrm{Ca}/\mathrm{Pe}$ becomes smaller, where Ca and Pe denote respectively the capillary and Peclet numbers, the axisymmetric mode becomes more dominant than azimuthal modes. They also found for flow inside the cylinder that the axisymmetric mode is always the most unstable although azimuthal modes can be excited. In addition, for the same values of parameters, azimuthal modes excited for flow inside the cylinder are fewer than those for flow outside the cylinder. Our analysis shall focus on the axisymmetric instability. As we shall discuss, for parameters of our interest, studying the axisymmetric instability appears to be a rational approach to our problem in view of its greater importance than azimuthal modes according to Ref. 17.

The above-mentioned studies focused on the stability of a single fluid layer under thermocapillary influences. In Ref. 16, the base flow is driven by a prescribed axial thermocapillary force, and exerts a stress on the interface. The thermocapillary influence comes from both the basic flow and the perturbation temperature field. In Ref. 17, the base flow is a freely falling flow, and hence the interface is stress-free. Thermocapillary effects in this study are only attributed to the perturbation temperature field. The current study is different from these early works. The most apparent difference is that our system is a two-fluid flow, rather than a single-layer flow, which clearly makes base flows behave differently. More importantly, the stability features are further influenced by the contrast of fluids' mechanical/thermal properties, which is absent in single-fluid systems. Our approach is also different from Refs. 16 and 17. In contrast to these studies in which stabilities were examined numerically, we develop an asymptotic theory to examine the stability of a CAF in the thin-annulus limit. This can provide a more lucid way to reveal relevant physics. Despite the above differences, some of our results still can be compared qualitatively with those in these early studies, as we shall discuss in detail in Sec. VI. Furthermore, as we shall demonstrate, since our thin-film CAF study covers a wide range of parameters, it is also likely to extend the applicability to gas-liquid systems (e.g., trickle beds).

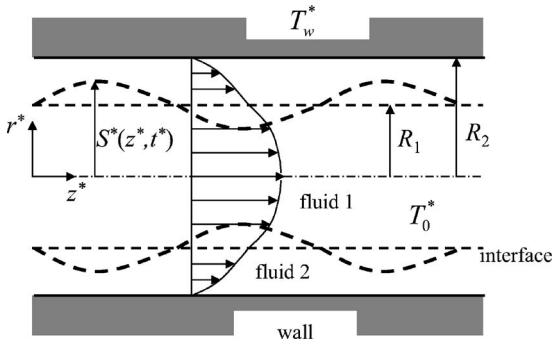

FIG. 1. Geometry of a core-annular flow.

The paper is organized as follows. We begin with the base state, governing equations, and boundary conditions in Sec. II. In Sec. III, we establish two different sets of scalings and identify dominant instability mechanisms. The respective leading order linear stability analysis is outlined for each scaling case in Sec. IV. The extension to the weakly nonlinear regime is carried out in Sec. V. We compare our results with previous studies in Sec. VI. Application of the present study is discussed in Sec. VII. Concluding remarks are made in Sec. VIII.

II. BASE STATE, GOVERNING EQUATIONS, AND BOUNDARY CONDITIONS

Consider two immiscible, incompressible, Newtonian fluids flowing axisymmetrically in a core-annular arrangement in a straight tube with radius R_2. The interface is given by $r^*=S^*(z^*,t^*)$. Fluid 1 of viscosity μ_1 occupies the core region $0\leqslant r^*\leqslant S(z^*,t^*)$. Fluid 2 of viscosity μ_2 fills the annular region $S^*(z^*,t^*)\leqslant r^*\leqslant R_2$. Densities of the core and the annular fluids are denoted by ρ_1 and ρ_2, respectively. The temperatures of the tube wall and the core fluid are maintained at T_w^* and T_0^*, respectively. See Fig. 1. Velocity fields $\mathbf{v}^*=(u^*,0,w^*)$ are expressed in terms of the cylindrical coordinates (r^*,ϕ^*,z^*). Let $r^*=R_1$ be the undisturbed interface. The base flows are driven by a constant pressure gradient $\nabla^* p^*=-F\underline{e}_{z^*}$ with $F>0$. We choose R_1 as the characteristic length. With the centerline velocity $W_0=F[R_1^2(\mu_2-\mu_1)$

$+R_2^2\mu_1]/(4\mu_1\mu_2)$ as the characteristic velocity scale, pressure and time can be then scaled with $\mu_1 W_0/R_1$ and R_1/W_0, respectively. It is also convenient to introduce the viscosity ratio $m=\mu_2/\mu_1$ and the radius ratio $a=R_2/R_1$. We write the base flows in the dimensionless form as follows:

$$\bar{W}(r) = 1 - \frac{mr^2}{(a^2+m-1)} \text{ for } 0 \leqslant r \leqslant 1,$$

$$\bar{w}(r) = \frac{(a^2-r^2)}{(a^2+m-1)} \text{ for } 1 \leqslant r \leqslant a, \tag{1}$$

$$[\bar{p}] = \frac{1}{\mathrm{Ca}},$$

where $[\cdot]=(\cdot)_1-(\cdot)_2$, $\mathrm{Re}_1=\rho_1 W_0 R_1/\mu_1$ and $\mathrm{Ca}=\mu_1 W_0/\sigma_0^*$ denote the Reynolds number and the capillary number, respectively, and σ_0^* is the interfacial tension for the base state.

As for the base-state temperature field, we treat the core fluid as an ambient phase with a constant temperature. That is, the energy conveyed by the core is transmitted across the fluid-fluid interface into the annulus, or vice versa. This enables us to apply the Newton heat condition $k_f T_{r^*}^* = h(T^* - T_0^*)$ at the interface $r^*=R_1$, where h and k_f are the heat transfer coefficient and the thermal conductivity of the annular layer, respectively. This condition is generally appropriate at the boundary where a liquid is in contact with an ambient phase (usually a gas stream) that is well mixed or moves sufficiently fast. Its basis is briefly provided below.

Since the annular thickness is thin compared to the tube's radius as in most of the CAF applications, conduction dominates the heat transfer in the film. For a sufficiently fast core flow, the Peclet number Pe could be large enough so that the thermal boundary layer becomes sufficiently thin. In this case, as the core fluid with a constant temperature enters a pore, its temperature remains almost uniform outside the thin thermal boundary layer. Because the thermal boundary layer grows slowly in the streamwise direction for large Pe, the core temperature in this long entrance region can be approximated as a uniform profile before it equilibrates the wall or reaches a fully developed state. In this region, the application of the Newton heat condition could be appropriate. This will also be justified later using scaling arguments in Sec. III.

With the Newton heat condition applied at the interface, we normalize the temperature by $T=(T^*-T_0^*)/\Delta T^*$ with $\Delta T^* = T_w^* - T_0^*$, and obtain the following basic temperature profile for each fluid:

$$\bar{T} = 0 \text{ for } 0 \leqslant r \leqslant 1,$$

$$\bar{T}(r) = 1 + \frac{\mathrm{Bi}}{1+\mathrm{Bi}\ln a}\ln\left(\frac{r}{a}\right) \text{ for } 1 \leqslant r \leqslant a, \tag{2}$$

where $\mathrm{Bi}=hR_1/k_f$ is the Biot number.

For a dynamical system, the nondimensional equations of motion for each fluid are governed by the continuity and the Navier-Stokes equations:

$$\frac{1}{r}(ru)_r + w_z = 0, \tag{3}$$

$$\chi_i \mathrm{Re}_1(w_t + uw_r + ww_z) = -p_z + m_i\nabla^2 w, \tag{4a}$$

$$\chi_i \mathrm{Re}_1(u_t + uu_r + wu_z) = -p_r + m_i\left(\nabla^2 u - \frac{u}{r^2}\right), \tag{4b}$$

where $\chi_i=\rho_i/\rho_1$ is the density ratio and $m_i=\mu_i/\mu_1$ $(i=1,2)$. The system is subject to the following boundary conditions. The velocities vanish on the wall:

$$w_2 = u_2 = 0 \text{ at } r = a. \tag{5}$$

Velocities are continuous at the interface:

$$[w] = 0,\ [u] = 0 \text{ at } r = S(z,t). \tag{6}$$

At the interface $r=S(z,t)$, the tangential stress and normal stress conditions are

$$\frac{1}{(1+S_z^2)}[m_i((w_r+u_z)(1-S_z^2)+2(u_r-w_z)S_z)] = \frac{1}{\mathrm{Ca}}\sigma_z. \tag{7}$$

$$-[p - 2m_i u_r - (-p + 2m_i w_z)S_z^2 + 2m_i(u_r+w_z)S_z] = \frac{\sigma(T)}{\mathrm{Ca}}\left(S_{zz} - \frac{1}{S}(1+S_z^2)\right)(1+S_z^2)^{-3/2}. \tag{8}$$

The dependence of the interfacial tension on temperature is assumed to be linear:

$$\sigma = 1 - ET, \tag{9}$$

where $E=-(\Delta T^*/\sigma_0^*)(\partial\sigma^*/\partial T^*)_{T_0^*}$ is a dimensionless parameter that reflects the change in the interfacial tension in response to the temperature variation. $E>0$ (<0) corresponds to the system with the wall warmer (cooler) than the core fluid, viz., $\Delta T^*>0$ (<0). At the interface, the kinematic condition is also required:

$$u = S_t + wS_z \text{ at } r = S(z,t). \tag{10}$$

We finally require the regularity of the core flow at the centerline:

$$u_1 = w_{1r} = 0 \text{ at } r = 0. \tag{11}$$

As for the heat transfer problem, we assume that the core temperature remains constant for all times. This is only valid when the annular thickness is thin and Pe is large, as we shall justify *a posteriori*. The heat transfer equation for the annular layer is

$$T_t + uT_r + wT_z = \frac{\lambda}{\mathrm{Pe}}\nabla^2 T, \tag{12}$$

where $\mathrm{Pe}=W_0R_1/\alpha_T$ is the Peclet number, and α_T is the thermal diffusivity of the core and its ratio to that of the annulus is denoted by λ. The boundary conditions are

$$T = 1 \text{ at } r = a, \tag{13}$$

$$\frac{(T_r - S_z T_z)}{(1+S_z^2)^{1/2}} = \mathrm{Bi}T \text{ at } r = S(z,t). \tag{14}$$

The left-hand side of (14) is just $-\mathbf{n}\cdot\nabla T$ from conduction in the annulus where $\mathbf{n}$ is the unit normal pointing towards the core.

III. SCALING ANALYSIS

To asymptotically examine the stability of the base state in the thin-annulus limit, we follow an approach similar to Georgiou *et al.*[5] and Papageorgiou *et al.*[7] We first carry out a scaling analysis to identify the dominant instability mechanisms and to estimate the scales of perturbation quantities. We then expand the governing equations and boundary conditions with these perturbation quantities to formulate the leading order stability problem. We begin with the linear stability analysis and later extend it to the weakly nonlinear regime.

Let ε be the ratio of the undisturbed annular thickness to the core radius. In the thin-film limit ($\varepsilon \ll 1$), a stretched film variable $y = 1-(r-1)/\varepsilon$ is introduced to separate the radial scales in the film and core. For $m = O(1)$, the leading order base flows for the film and the core yield, respectively,

$$\bar{w} = 2\varepsilon y/m \text{ and } \bar{W} = 1 - r^2. \tag{15}$$

The leading order basic temperature profile of the film is

$$\bar{T} = \frac{1 + B(1-y)}{1+B}. \tag{16}$$

Here, $B = \varepsilon\mathrm{Bi}$ can be regarded as the Biot number based on the film, and is assumed to be $O(1)$. Since B is proportional to the film thickness εR_1, if the film thickness is sufficiently thin, then strong conduction through the film could be comparable to the heat transfer through the ambient core. In addition, we are interested in nontrivial effects due to thermocapillarity. As we shall show, in both small and large B limits, thermocapillarity has no impact on the stability; the effects are manifested only when $B = O(1)$.

The system is perturbed by disturbances to the interface and the annular temperature field with the respective sizes of $\delta_1 (\ll \varepsilon)$ and $\delta_2 (\ll 1)$:

$$S(z,t) = 1 + \delta_1 \eta(z,t) \text{ and } T(r,z,t) = \bar{T} + \delta_2 \theta(r,z,t). \tag{17}$$

In estimating the scales of perturbation quantities, it is worth noticing that there are different mechanisms driving perturbation flows. For strong surface tensions or low Ca, capillary forces usually drive the flow in the film. On the other hand, when surface tensions are low or Ca is large, the flow can be solely driven by thermocapillary forces.

Let (w'', u'', p'') and (W'', U'', P'') denote the perturbation quantities for the annulus and the core, respectively. We first consider the capillary scaling for the film flow and check the consistency *a posteriori*. The perturbed film pressure is $p'' \sim \delta_1/\mathrm{Ca}$ from the normal stress condition (8). This capillary pressure drives the film flow through the axial momentum (4a) and the continuity (3), giving rise to $w'' \sim \varepsilon^2\delta_1/\mathrm{Ca}$ and $u'' \sim \varepsilon^3\delta_1/\mathrm{Ca}$. As for the core quantities, the continuity of axial velocities across the interface (6) and the lack of separation between the axial and radial length scales yield $W'' \sim \delta_1$, $U'' \sim \delta_1$, and $P'' \sim \delta_1$.

To gain further information about the relation between the relevant scalings, we examine the heat transfer condition (14) and the tangential stress condition (7) at the interface. The linearized form of (14) is

$$\bar{T}_{rr}|_{r=1}\delta_1\eta + \delta_2\theta_r|_{r=1} = \mathrm{Bi}(\bar{T}_r|_{r=1}\delta_1\eta + \delta_2\theta). \tag{18}$$

The first two terms reflect the effects of the perturbed conductive heat flux across the interface. The first term is due to the perturbed interface and has $O(\delta_1/\varepsilon)$ because of $\bar{T}_{rr}|_{r=1} = -\mathrm{Bi}/(1+\varepsilon\mathrm{Bi}) = O(\varepsilon^{-1})$. The second term is attributed to the perturbed film temperature and has $O(\delta_2/\varepsilon)$ in view of $\theta_r = -\varepsilon^{-1}\theta_y$ in the film. By noticing that $\mathrm{Bi} = \varepsilon^{-1}B = O(\varepsilon^{-1})$, the third term comes from the perturbation to the basic temperature and has $O(\delta_1/\varepsilon^2)$. The last term due to the perturbed film temperature field is $O(\delta_2/\varepsilon)$. Therefore, the leading order terms of (18) are all of them except the first one. Balancing the orders of these terms, we have

$$\delta_2 \sim \delta_1/\varepsilon. \tag{19}$$

We now inspect the interfacial tangential stress condition (7) to identify the relative importance of the viscous and thermocapillary stresses. The film and the core have viscous stresses $mw''_r = -\varepsilon^{-1}mw''_y \sim \varepsilon\delta_1/\mathrm{Ca}$ and $(W''_r + U''_z) \sim \delta_1$, respectively. The thermocapillary stress is $\sigma_z/\mathrm{Ca} = -\mathrm{Ma}\,\delta_2\theta_z \sim \mathrm{Ma}\,\varepsilon^{-1}\delta_1$, where $\mathrm{Ma} = E/\mathrm{Ca}$ denotes the Marangoni number. Assuming $\mathrm{Ma} = O(1)$, we balance the film viscous stress and the thermocapillary force, and arrive at $\mathrm{Ca} \sim \varepsilon^2$. In this case, both capillary and thermocapillary forces drive the perturbed film flow at leading order. The resulting scalings of the perturbed film flow become $p'' \sim \delta_1/\varepsilon^2$, $w'' \sim \delta_1$, and $u'' \sim \varepsilon\delta_1$. By checking the perturbed film pressure arising from the temperature-induced interfacial tension variation, we find $p'' \sim \delta_2 E/\mathrm{Ca} \sim \delta_1/\varepsilon$, which is of a higher order than the capillary pressure $p'' \sim \delta_1/\varepsilon^2$.

The above scalings are based on $\mathrm{Ma} = O(1)$ and $\mathrm{Ca} \sim \varepsilon^2$, where both thermocapillary and capillary forces are comparable. If $\mathrm{Ca} \ll \varepsilon^2$, capillarity dominates the instability and thermocapillarity is of a higher order correction. We are less interested in this case because it is equivalent to the limit in the absence of a base flow. On the other hand, for $\mathrm{Ca} \gg \varepsilon^2$, capillary forces are weak, therefore the thermocapillary stress becomes the sole force driving the perturbed film flow at leading order. In this situation, applying the tangential stress condition (7) yields $w'' \sim \varepsilon\delta_2\,\mathrm{Ma} \sim \delta_1\,\mathrm{Ma}$ and $u'' \sim \varepsilon^2\delta_2\,\mathrm{Ma} \sim \varepsilon\delta_1\,\mathrm{Ma}$. Therefore, we conclude that for $\mathrm{Ma} = O(1)$ and $\mathrm{Ca} \gtrsim \varepsilon^2$, the film velocities are $w'' \sim \delta_1\,\mathrm{Ma}$ and $u'' \sim \varepsilon\delta_1\,\mathrm{Ma}$. Now balancing u'' and S_t in the kinematic condition (10), we obtain a long time scale $\tau = \varepsilon t$, appropriate for capturing a nontrivial temporal evolution of the interface.

As we shall show in Sec. IV A, for $\mathrm{Ma} = O(1)$ and $\mathrm{Ca} \gtrsim \varepsilon^2$, the system's leading order stability is determined by the film flow; the core dynamics just respond passively to the film. This is deduced from the interfacial tangential stress condition (7) in that the core flow is of a higher order than both the film flow and thermocapillary effects. However, the core dynamics can be important if $\mathrm{Ma} \sim \varepsilon$ as a result of bal-

ancing the thermocapillary stress of $O(\mathrm{Ma}\,\varepsilon^{-1}\delta_1)$ and the core viscous stress of $O(\delta_1)$. As in Papageorgiou *et al.*,[7] the core flow contribution can also be included when the surface tension is moderately strong, viz., $\mathrm{Ca}\sim\varepsilon$, under which the capillary-driven film stress and the core stress are comparable. In this case, the perturbed film flow has $p''\sim\delta_1/\varepsilon$, $w''\sim\varepsilon\delta_1$, and $u''\sim\varepsilon^2\delta_1$. For $\mathrm{Ca}\gg\varepsilon$, since both the core viscous and thermocapillary forces shear the film flow at leading order, the corresponding scalings of the perturbed film velocities remain the same as those of the $\mathrm{Ca}\sim\varepsilon$ case. Notice that $\mathrm{Ma}\sim\varepsilon$ does not necessarily suggest small E since Ca could be sufficiently large. Now inspecting the interfacial evolution of the film for $\mathrm{Ma}\sim\varepsilon$ and $\mathrm{Ca}\gtrsim\varepsilon$, we find that the appropriate time scale is $\tau=\varepsilon^2 t$ in the frame moving with the basic interfacial velocity, viz., $z\to z-\bar{w}(1)t$. As for $\mathrm{Ca}\ll\varepsilon$ and $\mathrm{Ma}\sim\varepsilon$, capillary forces dominate the system's instability, and both thermocapillary and the core flow effects are higher order contributions. This case can be again treated as the no-flow limit, and is of less interest to the present study.

We now inspect the heat transfer equation (12) for the film. Its left-hand side is $O(\varepsilon\delta_2)$ at most while the conduction term is $O(\varepsilon^{-2}\,\mathrm{Pe}\,\delta_2)$ (provided that λ is O(1)). Therefore, conduction is more important than convection when $\varepsilon^3\,\mathrm{Pe}\ll 1$. For typical liquids, thermal diffusivity α_T is 10^{-4}–10^{-3} cm^2/s. The estimated Pe is thus $O(10)\sim O(10^2)$ for a flow speed of 1 cm/s in a capillary of 200 μm diameter. For $\varepsilon=0.1$, $\varepsilon^3\,\mathrm{Pe}\ll 1$ suffices to assure that the film heat transfer is dominated by conduction.

As for the heat transfer in the core, we have invoked the Newton heat condition for bringing the core influence into the problem. This condition is often applied to gas-liquid systems where the gas phase is kept at a constant temperature for all times. For liquid-liquid systems, however, the Newton condition can also be adequate under certain circumstances, which are discussed below. Since a long time scale has been introduced to the problem, the core heat transfer is governed by a quasisteady convective-conduction equation. For a sufficiently large Pe (but $\ll\varepsilon^{-3}$ to ensure that conduction prevails in the film as discussed earlier), there is a thin thermal boundary layer of (dimensional) thickness δ_T adjacent to the interface outside which the core heat transfer is dictated by convection. Since the interface is located in the proximity of the no-slip wall when the annulus is thin, the flow condition thereof is somehow between the shear-free and no-slip conditions. It seems rational to assume that $\delta_T/R_1\sim\mathrm{Pe}^{-n}$ with n ranging between 1/3 and 1, and that δ_T does not change appreciably with z within a long thermal entrance region. In the region outside δ_T, the core temperature can be approximately uniform, so that the Newton condition can, in principle, be applied at the outer edge of δ_T, which can be approximately written at the interface. Also, by writing the core conduction at the interface as $k_{\mathrm{core}}\partial T^*/\partial r^*\sim k_{\mathrm{core}}\Delta T_b^*/\delta_T\sim h\Delta T_b^*$ (k_{core} the core thermal conductivity and ΔT_b^* the bulk-interface temperature difference), we find $h\delta_T/k_{\mathrm{core}}\sim O(1)$, which is consistent with the scaling $B\sim O(1)$ mentioned earlier provided that $k_{\mathrm{core}}/k_f=O(1)$.

A further remark should be made concerning the development of the instability of interest. Recall that the heat transfer problem is based on the isothermal core so that the application of the Newton heat condition can be relevant. This requires the core fluid to have a constant temperature (e.g., a well-mixed gas core), or to move sufficiently fast to attain a suitably large Pe. For the latter case, the instability of interest should be more appropriate in a long thermal entrance region (while the flow is assumed to be fully developed). Knowledge of the thermal entrance length L_T associated with the present problem is still lacking. Nevertheless, since the core is surrounded by the thin annulus, it might not be unreasonable to assume that L_T here can be characterized in a way similar to the classical Graetz problem of a single fluid in a rigid tube, at least for large Pe. As such, we assume that $L_T\sim\mathrm{Pe}\,R_1$. In what follows, the fluid takes a time of $O(\mathrm{Pe}\,R_1/W_0)$ to reach the fully developed region. Since the interfacial instability develops within the time scale $R_1/(\varepsilon W_0)$ (for $\mathrm{Ca}\sim\varepsilon^2$) or $R_1/(\varepsilon^2 W_0)$ (for $\mathrm{Ca}\sim\varepsilon$), it demands that the time scale for developing the thermal boundary layer is much longer than the instability time scale, so that the occurrence of the instability is under the prescribed temperature and heat transfer conditions. That is, we need $\mathrm{Pe}\gg\varepsilon$ (for $\mathrm{Ca}\sim\varepsilon^2$) or $\mathrm{Pe}\gg\varepsilon^2$ (for $\mathrm{Ca}\sim\varepsilon$) (note that any scaling of L_T different from Pe would affect the subsequent discussion and the relevant scalings mentioned above). Since $\varepsilon^3\,\mathrm{Pe}\ll 1$ is also required for ensuring that conduction is dominant in the film, these constraints yield a range of Pe appropriate for the problem. As such, the rationale of the *ansatz* devised here can be established and realized.

In summary, we have derived two sets of scalings: (i) $\mathrm{Ma}\sim O(1)$ and $\mathrm{Ca}\gtrsim\varepsilon^2$ and (ii) $\mathrm{Ma}\sim\varepsilon$ and $\mathrm{Ca}\gtrsim\varepsilon$. The stability of the former is solely determined by the film while the latter further involves the coupling to the core dynamics. Since our stability analysis is based on lubrication theory in the annulus, it requires that $\varepsilon^3(\rho_2/\rho_1)\mathrm{Re}_1\ll m$ so that the film inertia can be neglected. Hence the results that follow are not limited to low Re_1, but valid for nonzero Re_1 as long as $\mathrm{Re}_1\ll m(\rho_1/\rho_2)\varepsilon^{-3}$. Furthermore, in light of the fact that the present analysis covers a wide range of parameters, it is also likely to be applicable to gas-liquid systems.

In the following section, we shall formulate the respective linear stability analysis for each scaling case described above.

IV. LEADING ORDER LINEAR STABILITY ANALYSIS

A. Ma$\sim O(1)$ and Ca$\gtrsim\varepsilon^2$

We focus on $\mathrm{Ca}\sim\varepsilon^2$ here since $\mathrm{Ca}\gg\varepsilon^2$ can be regarded as the large-Ca limit. Let $\mathrm{Ca}=\varepsilon^2\,\mathrm{Ca}_0$ with $\mathrm{Ca}_0=O(1)$. The film quantities can be expressed as

$$w=\bar{w}+\delta_1 w'+O(\varepsilon\delta_1),\quad u=\varepsilon\delta_1 u'+O(\varepsilon^2\delta_1),$$

$$p=\bar{p}+(\delta_1/\varepsilon^2)p'+O(\delta_1/\varepsilon),$$

$$T=\bar{T}+\varepsilon^{-1}\delta_1\theta+O(\delta_1). \tag{20a}$$

For the core,

$$P = \bar{P} + \delta_1 P' + O(\varepsilon\delta_1).$$

$$W = \bar{W} + \delta_1 W' + O(\varepsilon\delta_1), \quad U = \delta_1 U' + O(\varepsilon\delta_1), \tag{20b}$$

After substituting the above into Eqs. (2)–(14) and expanding them with respect to the base state, the leading order governing equations of the perturbed film flow become

$$u'_y = w'_z, \tag{21}$$

$$0 = -p'_z + m w'_{yy}, \tag{22a}$$

$$0 = -p'_y. \tag{22b}$$

The film flow field that satisfies no-slip and no-penetration conditions at the wall $y=0$ is

$$w' = \frac{1}{2m} p'_z y^2 + Ay, \tag{23a}$$

$$u' = \frac{1}{6m} p'_{zz} y^3 + \frac{1}{2} y^2 A_z, \tag{23b}$$

$$p' = p'(z,\tau). \tag{23c}$$

Here, A is determined by the leading order tangential condition at the interface:

$$m w'_y(y=1) = -\mathrm{Ma}\left(\frac{B}{1+B}\eta + \theta(y=1)\right)_z. \tag{24}$$

The film pressure p' is simply provided by capillarity from the normal stress at the interface:

$$p' = \frac{1}{\mathrm{Ca}_0}(\eta + \eta_{zz}). \tag{25}$$

The leading order kinematic condition becomes

$$u' = \eta_\tau. \tag{26}$$

Here we have invoked a long time scale $\tau=\varepsilon t$ in the frame moving with the basic interfacial velocity $\bar{w}(y=1)$.

For $\varepsilon^3\,\mathrm{Pe} \ll 1$ and $\lambda = O(1)$, the leading order heat transfer in the film is governed by the steady-state conduction equation:

$$\theta_{yy} = 0, \tag{27}$$

with the boundary conditions:

$$\theta(y=0) = 0, \tag{28}$$

$$-\theta_y = B\left(\frac{B}{1+B}\eta + \theta\right) \quad \text{at } y = 1. \tag{29}$$

Equations (21)–(29) suffice to determine the perturbed film flow without need of the core flow solution. As such, we first solve the perturbed film flow field using Eqs. (21)–(25) in terms of η and θ. We then solve θ using Eqs. (27)–(29) and substitute it into the film flow field in terms of η. As a result, the Marangoni-stress term in Eq. (24) becomes

$$-\mathrm{Ma}\left(\frac{B}{1+B}\eta + \theta(y=1)\right)_z = -\mathrm{Ma}\frac{B}{(1+B)^2}\eta_z. \tag{30}$$

Here, $B/(1+B)^2\eta$ can be regarded as the variation of the interfacial temperature due to the interfacial perturbation. This can be seen more directly by considering the temperature field in the film: $T=[1+B(y_s-y)]/(1+By_s)$, where $y_s = 1-\varepsilon^{-1}\delta_1\eta$ is the dynamical film thickness normalized by the mean, which satisfies $T_{yy}=0$ subject to $T(y=0)=0$ and $T_y|_{y=y_s} = -BT(y=y_s)$. At the deflected interface $y=y_s$, the temperature is $T=1/(1+By_s) \approx 1/(1+B)+B/(1+B)^2\varepsilon^{-1}\delta_1\eta$, in which the η term reflects the temperature variation with respect to the basic interfacial temperature.

By applying the kinematic condition (26), we finally arrive at the following evolution equation for the interface that governs the system's leading order linear stability:

$$\eta_\tau + \frac{1}{3m\,\mathrm{Ca}_0}(\eta_{zz} + \eta_{zzzz}) + \frac{\mathrm{Ma}\,B}{2m(1+B)^2}\eta_{zz} = 0. \tag{31}$$

Recall that we have changed frame of reference with respect to the base interfacial velocity and a long time scale, viz., $z \to z - \bar{w}(1)t$ and $\tau=\varepsilon t$. The second term of Eq. (31) is the usual capillarity and the third term reflects the thermocapillary effects. Note that both $m\,\mathrm{Ca}_0$ and Ma/m in Eq. (31) involve only the viscosity of the fluid film. Further notice that the form of Eq. (31) is identical to that of a stationary system. That is, the linear stability is independent of the base flow. As we shall demonstrate later, although a base flow does not affect the linear stability, it plays a critical role in influencing the nonlinear dynamics.

We now perform a normal mode analysis on Eq. (31): $\eta = \hat{\eta}\exp(ikz + s\tau)$, where k is the wave number of the disturbance and s is the complex growth rate. The system is unstable (stable) when the real part of s, $s_r > 0$ (<0). The resulting normal-mode form of Eq. (31) becomes

$$s = \frac{1}{3m\,\mathrm{Ca}_0}(k^2 - k^4) + \frac{\mathrm{Ma}\,B}{2m(1+B)^2}k^2. \tag{32}$$

In the limit of $\mathrm{Ma}=0$ (an isothermal film) or $B=0$ ($B \ll O(1)$ or a nearly insulated film), Eq. (32) agrees with the isothermal result of Georgiou *et al.*[5] As $B \to \infty$ [i.e., $B \gg O(1)$], the basic film temperature equilibrates the isothermal core, hence making no impact on the stability.

For nonzero B, Eq. (32) indicates that $\mathrm{Ma} > 0$ (<0) makes the system more (less) unstable compared to the pure capillary instability ($\mathrm{Ma}=0$), as depicted in Fig. 2. The mechanism of thermocapillary stability/instability due to surface waves has been explained previously.[18] We include it here for completeness as well as for illustrating its interplay with the capillary instability. Consider a system with a heated wall ($\mathrm{Ma} > 0$). As revealed by Eq. (30), an interfacial disturbance causes the interface crests (the thinnest portions of the film) to be warmer than the interface troughs (the thickest portions of the film). The induced thermocapillary forces in turn pull the fluid toward the troughs, giving rise to a growth of the interface and hence destabilizing the system. This thermocapillary destabilization, which works for all k ($\ll \varepsilon^{-1}$), thus exaggerates the longwave instability of capillarity. On

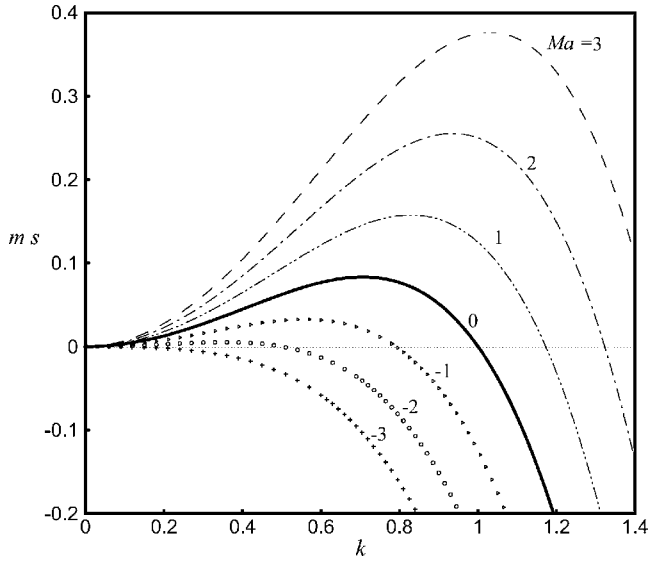

FIG. 2. Effects of Ma on the growth rates of Eq. (32). $\mathrm{Ca}_0=1.0$, $B=1.0$.

the other hand, since the $\mathrm{Ma}>0$ thermocapillary destabilization is compromised by the short wave capillary stabilization, the critical wave number $k_c=[1+3B/2(1+B)^2\,\mathrm{Ma}\,\mathrm{Ca}_0]^{1/2}$ shifts towards a larger value, and so does the wave number $k_{\max}=[2+3B/(1+B)^2\,\mathrm{Ma}\,\mathrm{Ca}_0]^{1/2}$ corresponding to the maximum growth rate. On the contrary, for $\mathrm{Ma}<0$, thermocapillarity is stabilizing, making both k_c and $k_{\max}$ smaller.

For $\mathrm{Ma}<0$ the stability depends on the competition between the thermocapillary stabilization and the capillary destabilization. This can be recognized by the k^2 term of Eq. (32). Thermocapillarity can completely suppress the capillary instability if $\mathrm{Ma}<\mathrm{Ma}^*\equiv-2(1+B)^2/(3B\,\mathrm{Ca}_0)$, which is confirmed by Fig. 2 ($\mathrm{Ma}^*=-8/3$). Alternatively, for a given flow condition there exists a critical temperature difference, $\Delta T^*=T-T=2/(3\mu W_0)(\partial\sigma^*/\partial T^*)^{-1}_{T_0^*}(1+B)/(B\,\mathrm{Ca}_0)$, below which the system is stable. That is, the higher tension (the smaller Ca) is, the higher temperature the core fluid required to stabilize the system, provided that all other fluid properties do not vary much in a range of the temperature variation.

B. $\mathrm{Ma}\sim\varepsilon$ and $\mathrm{Ca}\gtrsim\varepsilon$

We again focus on $\mathrm{Ca}\sim\varepsilon$ in order to retain both capillary and thermocapillary effects at leading order. Let $\mathrm{Ma}=\varepsilon M_0$ and $\mathrm{Ca}=\varepsilon\,\mathrm{Ca}_0$, where both M_0 and Ca_0 are $O(1)$. The expansions of the film quantities are

$$w=\bar{w}+\varepsilon\delta_1 w'+O(\varepsilon^2\delta_1),\quad u=\varepsilon^2\delta_1 u'+O(\varepsilon^3\delta_1),$$
$$p=\bar{p}+(\delta_1/\varepsilon)p'+O(\delta_1),\tag{33}$$
$$T=\bar{T}+\varepsilon^{-1}\delta_1\theta+O(\delta_1).$$

Those quantities of the core remain the same as (20b). The resulting leading order governing equations and boundary conditions for the film are the same as those of the preceding case except for the interfacial tangential stress condition (24), which now becomes

$$mw_y'(y=1)=-M\left(\frac{B}{1+B}\eta+\theta(y=1)\right)_z-(W_r'+U_z')_{r=1}.\tag{34}$$

Here an additional contribution from the perturbed core shear stress comes into play. The leading order governing equations for the core become

$$\frac{1}{r}(rU')_r+W_z'=0,\tag{35a}$$
$$\mathrm{Re}_1[-2rU'+(1-r^2)W_z']=-P_z'+\nabla^2W',\tag{35b}$$
$$\mathrm{Re}_1(1-r^2)U_z'=-P_r'+\left(\nabla^2U'-\frac{U'}{r^2}\right).\tag{35c}$$

Note that the time-derivative terms are of higher order effects because the time scale is $O(\varepsilon^{-2})$ here. The boundary conditions for Eqs. (35) include the regularity of velocities along the axis of symmetry as in (11), and the continuity of velocities at the interface (6). The leading order form of the latter is

$$W'(r=1)=2\left(1-\frac{1}{m}\right)\eta,\quad U'(r=1)=0.\tag{36}$$

Following the derivation procedures outlined by Papageorgiou *et al.*,[7] the core dynamics can be either expressed in terms of modified Bessel functions for $\mathrm{Re}_1\ll1$ (i.e., Stokes flow), or represented by Kummer functions for $\mathrm{Re}_1=O(1)$. In the former, the core dynamics are merely dispersive to the stability;[7] thus we pay attention to the latter.

For $\mathrm{Re}_1=O(1)$, we derive the following interfacial evolution equation that governs the leading order linear stability of the system:

$$\eta_\tau+\frac{1}{3m\,\mathrm{Ca}_0}(\eta_{zz}+\eta_{zzzz})+\frac{M_0B}{2m(1+B)^2}\eta_{zz}-\frac{i}{2\pi m}\left(1-\frac{1}{m}\right)\int_{-\infty}^{\infty}N_K(k)\int_{-\infty}^{\infty}\eta(x,\tau)e^{ik(z-x)}dxdk=0,\tag{37}$$

where

$$N_K(k)=\frac{I_1(k)e^{-\lambda}M(\Lambda,2,2\lambda)}{N_1(k)I_0(k)-N_2(k)I_1(k)}$$

with

$$\lambda=\frac{1}{2}(k\,\mathrm{Re}_1)^{1/2}e^{-i\pi/4},\quad \Lambda=1+k^2/8\lambda-\lambda/2,$$

$$N_1(k)=\int_0^1[I_1(k)K_1(kr)-I_1(kr)K_1(k)]r^2e^{-\lambda r^2}M(\Lambda,2,2\lambda r^2)dr,$$

$$N_2(k) = \int_0^1 [I_0(k)K_1(kr) + I_1(kr)K_0(k)]r^2 e^{-\lambda r^2} M(\Lambda,2,2\lambda r^2)dr.$$

The functions I and K represent modified Bessel functions of various orders, and $M(\Lambda,2,x)$ denotes the confluent hypergeometric function (the Kummer function). The last term of Eq. (37) reflects a nonlocal term arising from the core flow via viscosity stratification. Using normal modes, Eq. (37) yields

$$s = \frac{1}{3m\,\mathrm{Ca}_0}(k^2 - k^4) + \frac{M_0 B}{2m(1+B)^2}k^2 + \frac{i}{m}\left(1 - \frac{1}{m}\right)N_K(k, \mathrm{Re}_1). \tag{38}$$

For $M_0=0$, Eq. (38) again reduces to the isothermal result of Georgiou *et al.*[5] The thermocapillary term is the same as that of Eq. (32) (albeit different scaling of Ma is used here). The core inertia acts to stabilize (destabilize) for $m<1$ (>1).[5] To elucidate the combined effects of both thermocapillarity and core inertia on the stability in more detail, we utilize a long wavelength analysis below. The $k\to 0$ asymptote of Eq. (38), with the aid of $N_k=-4k-ik^2\,\mathrm{Re}_1/12+O(k^3)$, yields

$$s = -\frac{4i}{m}\left(1 - \frac{1}{m}\right)k + \left[\frac{1}{3m\,\mathrm{Ca}_0} + \frac{M_0 B}{2m(1+B)^2} + \frac{1}{12m}\left(1 - \frac{1}{m}\right)\mathrm{Re}_1\right]k^2 + O(k^3). \tag{39}$$

As a result, the long-wave instability is determined at $O(k^2)$. For $m>1$, the system is unstable for $M_0>0$, but the system can be stable for $M_0>0$ if $M_0B/(2(1+B)^2)<-1/(3\,\mathrm{Ca}_0) - \frac{1}{12}(1-1/m)\mathrm{Re}_1$. On the other hand, for $m<1$ and $M_0>0$, there exists a critical $\mathrm{Re}_1, \mathrm{Re}_1^*$, beyond which the system is stabilized by the core inertia:

$$\mathrm{Re}_1^* = \left(\frac{4}{\mathrm{Ca}_0} + \frac{6M_0B}{(1+B)^2}\right)\left(\frac{1}{m} - 1\right)^{-1}. \tag{40}$$

Equation (40) suggests that for $m<1$, thermocapillarity destabilizes the system in a manner in which Re_1^* increases with increasing M_0. That is, the warmer the wall (or the cooler the core), the higher Re_1 required to stabilize the system.

In light of the above, we show the effects of Re_1 on the growth rates in Fig. 3. As expected, increasing Re_1 (and hence the core inertia) tends to increase the growth rates for $m=2>1$ while the opposite occurs for $m=0.5<1$. The long-wave growth rates agree with the $k\to 0$ asymptote (39), as illustrated for $m=0.5$. The result for $m=0.5$ suggests that the critical Re_1^* occurs in a range between 4 and 6, which is consistent with the estimate using Eq. (40): $\mathrm{Re}_1^*=5.5$. We also numerically evaluate Re_1^* directly from Eq. (38), and find it in excellent agreement with Eq. (40), as shown by Fig. 4. Therefore, the approximation provided by Eq. (40) for finding Re_1^* is confirmed and adequate.

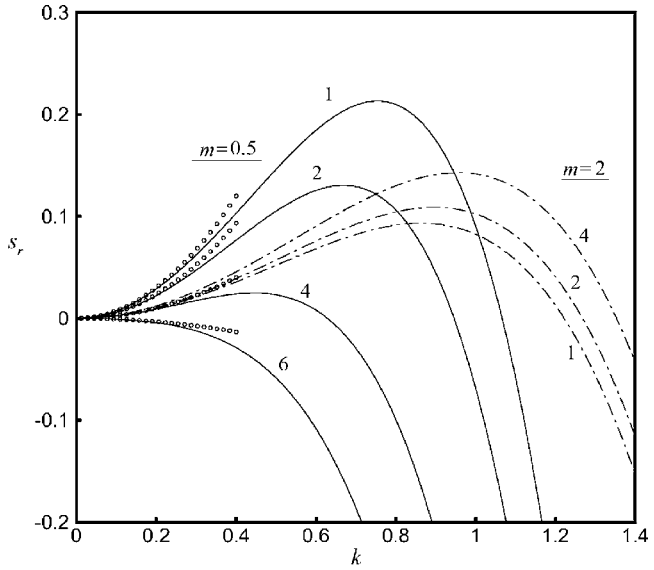

FIG. 3. The growth rate curves of Eq. (38). $\mathrm{Ca}_0=1.0$, $M_0=1$, $B=1.0$. $m=0.5$ (solid lines) with the $k\to 0$ asymptote Eq. (39) (symbols), $m=2$ (dashed-dotted lines). For a given m, growth rate curves with different Re_1 are plotted.

V. WEAKLY NONLINEAR STABILITY ANALYSIS

In this section, we extend the linear analysis to the weakly nonlinear regime. As shown above, thermocapillarity induces an instability when the wall is warmer than the core fluid. This exacerbates the instability when the capillary instability is present. When the core fluid is warmer than the wall, even though thermocapillarity is stabilizing, it may not be sufficiently strong to suppress the capillary instability. As the amplitude of the interface becomes gradually larger, the fate of the interface lies on the persistence of the instability. It involves the interplay between thermocapillarity, the short-wave capillary stabilization and the nonlinear wave steepen-

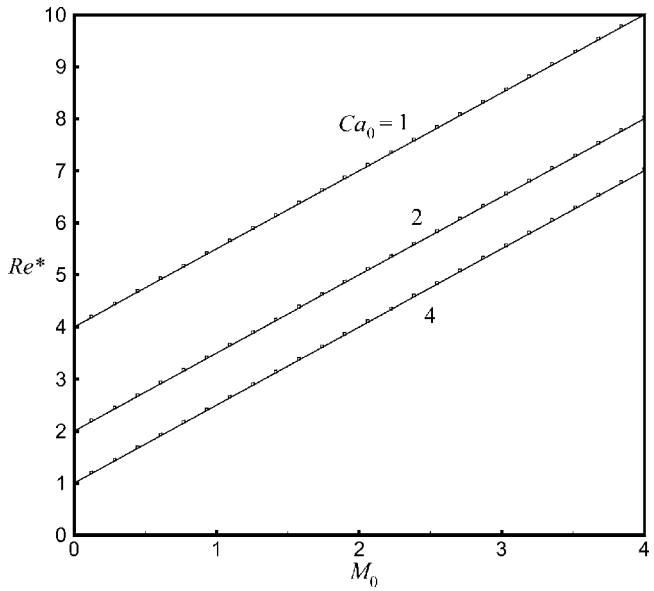

FIG. 4. The dependence of the critical Reynolds number Re^* on M_0. $m=0.5$. $B=1.0$. Solid lines are from Eq. (40). Symbols are the numerical results using Eq. (38).

ing. If the instability can be indeed arrested within the weakly nonlinear regime, another question will be raised concerning how thermocapillary effects modify the spatiotemporal features of the interfacial dynamics. These issues are addressed in this section. The respective weakly nonlinear analyses for (i) $\mathrm{Ma}\sim O(1)$ and $\mathrm{Ca}\gtrsim\varepsilon^2$ and (ii) $\mathrm{Ma}\sim\varepsilon$ and $\mathrm{Ca}\gtrsim\varepsilon^2$ are performed below.

A. $\mathrm{Ma}\sim O(1)$ and $\mathrm{Ca}\gtrsim\varepsilon^2$

We assume that interfacial deflections are much smaller than the film thickness, i.e., $\delta_1\ll\varepsilon$. Following similar procedures outlined in IV.A, the corresponding weakly nonlinear evolution equation for Eq. (31) can be derived below:

$$\eta_\tau-\frac{2}{m}\left(\frac{\delta_1}{\varepsilon}\right)\eta\eta_z+\left\{\left[1-3\left(\frac{\delta_1}{\varepsilon}\right)\eta\right](\alpha\eta_z+\gamma\eta_{zzz})\right\}_z=0, \tag{41}$$

where $\alpha=\mathrm{Ma}\,B/(2m(1+B)^2)+1/(3m\,\mathrm{Ca}_0)$ and $\gamma=1/(3m\,\mathrm{Ca}_0)$. The nonlinear effects appear $O(\delta_1/\varepsilon)$ and come from two parts. The first $O(\delta_1/\varepsilon)$ term is the Kuramoto-Sivashinsky (KS) nonlinearity, and arises from the perturbation to the basic interfacial velocity. The second is due to the variation of the film thickness $[1-(\delta_1/\varepsilon)\eta]^3$, and appears to be a modification to the KS equation. Notice that the constraint for the interfacial amplitude $\delta_1|\eta|_{\max}\ll\varepsilon$ has to be checked *a posteriori* for ensuring the validity of the weakly nonlinear analysis. This is because even though $\delta_1|\eta|_{\max}$ remains bounded, it could be so large such that terms that have been neglected become important. In this scenario, the equation is no longer appropriate to describe the dynamics; this happens long before the CAF arrangement is threatened. The dynamics should then be examined by a strongly nonlinear analysis[8] or direct numerical simulations.[9,10]

We now perform numerical simulations of Eq. (41). We choose $\delta_1=0.2\varepsilon$ and the initial condition $\eta(z,\tau=0)=0.01\cos(kz)$. For a given set of parameters, the wave number k of the initial disturbance is chosen as $k=(\alpha/2\gamma)^{1/2}$ corresponding to the maximum linear growth rate. We apply the Fourier spectral method to decompose (41) into a coupled set of ordinary differential equations for the time-dependent coefficients of Fourier modes. These equations are then solved using Gear's method. A typical number of Fourier modes is 32, which is sufficient for capturing the detailed features of the spatial evolution.

We first examine the interfacial evolution for the isothermal case $\alpha=\gamma$. In this case, the dynamics are determined by the relative strength of capillarity to the base-flow wave steepening (the second term of (41)), depending on the magnitude of α. When $\alpha=O(1)$, capillary forces are comparable to the base flow effects. This situation is illustrated by $\alpha=\gamma=1.0$, and the resulting evolution of the interface is shown in Fig. 5(a). At $\tau=20$, the interface trough has reached an amplitude of $\delta_1|\eta|_{\max}\sim0.6\varepsilon$. It clearly violates the weakly nonlinear constraint, which manifests the persistence of the instability. Apparently, the subsequent dynamics of such a growing interface cannot be realized by the present weakly nonlinear analysis; one has to account for strongly nonlinear effects to see if the film ruptures or the core snaps. On the other hand, when $\alpha<O(1)$, the capillary instability is relatively weak, so the base flow becomes more effective in steepening the wave. The weakly nonlinear saturation of the instability could occur when the long-wave destabilization η_{zz} is comparable to nonlinear effects, viz., $\alpha\leqslant\delta_1/\varepsilon$. This case is illustrated by $\alpha=\gamma=0.2$ and its interfacial evolution is shown in Fig. 5(b). The interface growth instability is indeed confined within the weakly nonlinear regime as evidenced by $\delta_1|\eta|_{\max}\sim0.1\varepsilon$. In fact, for small α [$\leqslant\delta_1/\varepsilon$ but $\geqslant O(\varepsilon)$ here], it can be shown that (41) can be reduced to the Kuramoto-Sivashinsky (KS) equation. It is borne out by the observation

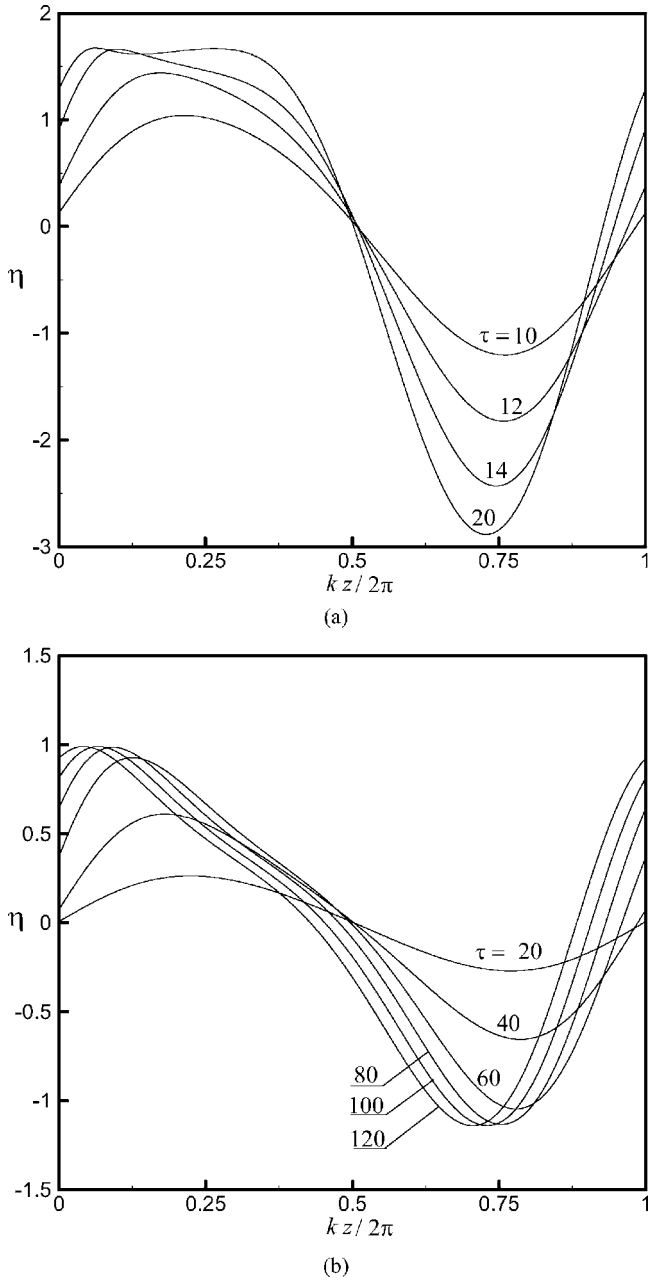

FIG. 5. Spatiotemporal evolutions of the weakly nonlinear interfacial equation (41) under isothermal conditions. $\delta_1=0.2\varepsilon$. (a) $\alpha=\gamma=1.0$. At $\tau=20$, the interface trough has reached an amplitude of $\delta_1|\eta|_{\max}\sim0.6\varepsilon$, which is beyond the weakly nonlinear regime. (b) $\alpha=\gamma=0.2$. The instability is saturated in the weakly nonlinear regime, as indicated by $\delta_1|\eta|_{\max}\sim0.1\varepsilon$.

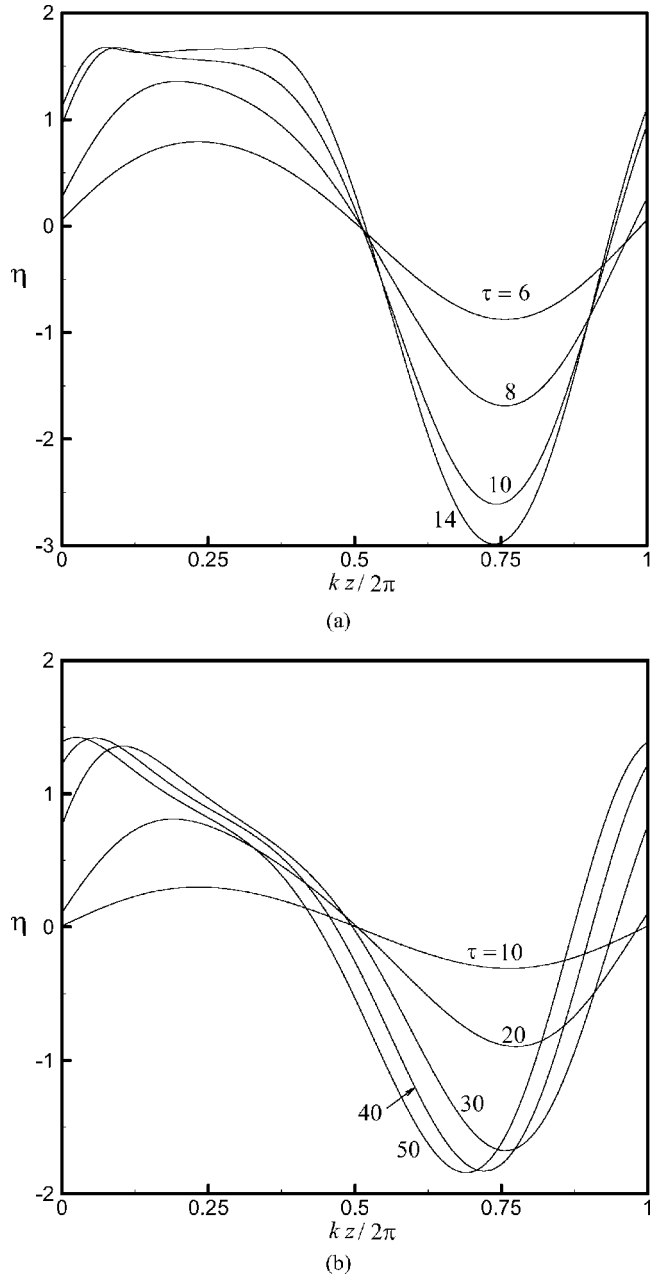

FIG. 6. Spatiotemporal evolutions of the weakly nonlinear interfacial equation (41) with the warmer wall. $\delta_1=0.2\varepsilon$. (a) $\alpha=1.2$, $\gamma=1.0$. The dynamics are beyond the weakly nonlinear regime because of $\delta_1|\eta|_{\max}\sim 0.6\varepsilon$ for the interface trough at $\tau=14$. (b) $\alpha=0.3$, $\gamma=0.2$. The weakly nonlinear analysis is almost invalid, as indicated by $\delta_1|\eta|_{\max}\sim 0.4\varepsilon$ for the interface trough.

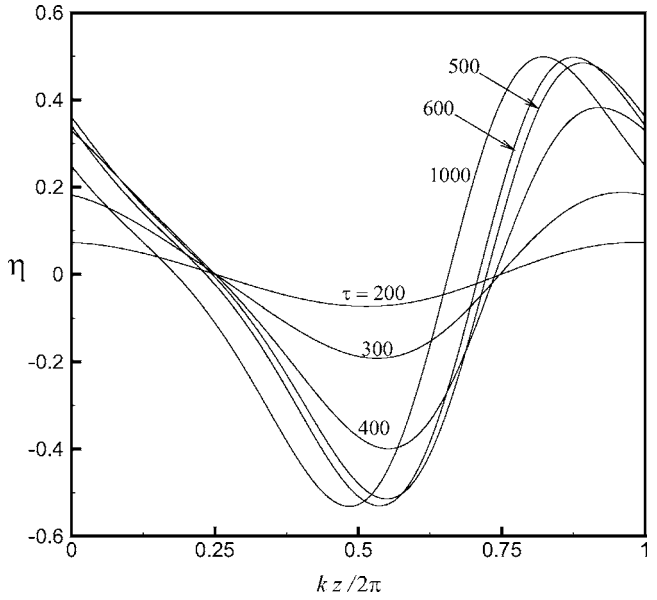

FIG. 7. Spatiotemporal evolutions of the weakly nonlinear interfacial equation (41) with the cooler wall. $\delta_1=0.2\varepsilon$, $\alpha=0.2$, $\gamma=1.0$. A slowly growing interface caused by the Marangoni-suppressed capillary instability can be arrested within the weakly nonlinear regime, as evidenced by $\delta_1|\eta|_{\max}<0.1\varepsilon$.

in Fig. 5(b) that the spatial evolution resembles that of the KS equation. The above results for isothermal systems also agree qualitatively with Kerchman.[8]

In the case of $\mathrm{Ma}>0$ (warmer walls) or $\alpha>\gamma(>0)$, the instability is enhanced by thermocapillarity. It is clear that for $\alpha=O(1)$ the instability will be magnified beyond the weakly nonlinear regime, as shown by Fig. 6(a). For $\alpha<O(1)$, however, while it is possible to have weakly nonlinear saturation under the isothermal condition [Fig. 5(b)], thermocapillarity could stimulate the interface growth so that the amplitude could have a size beyond the weakly nonlinear regime although it remains bounded. This scenario is illustrated by $\alpha=0.3$ and $\gamma=0.2$, as shown in Fig. 6(b). The result indicates that the evolution is beyond the validity of the weakly nonlinear regime in view of $\delta_1|\eta|_{\max}\sim 0.4\varepsilon$ for the interface trough.

As for $\mathrm{Ma}<0$ (cooler walls) or $\alpha<\gamma$, we are more interested in the case of $\alpha>0$ since $\alpha<0$ always makes the system stable. If α is not sufficiently small compared to γ, the instability is dominated by capillarity and its weakly nonlinear saturation is again not attainable, similar to the result shown in Fig. 6(b). When α is much smaller than γ, with stabilizing effects being much stronger than destabilizing effects, it is likely that the interface growth can be confined within the weakly nonlinear regime. This scenario is illustrated by the case with $\alpha=0.2$ and $\gamma=1.0$ (Fig. 7). It shows that the instability is indeed saturated within the weakly nonlinear regime, as evidenced by $\delta_1|\eta|_{\max}<0.1\varepsilon$.

B. $\mathrm{Ma}\sim\varepsilon$ and $\mathrm{Ca}\gtrsim\varepsilon$

As in the previous study,[7] we find that $\delta_1\sim\varepsilon^2$ is appropriate for the weakly nonlinear analysis in this case. The corresponding weakly nonlinear interfacial evolution equation is derived as follows:

$$\eta_\tau-\frac{2}{m}\eta\eta_z+\frac{1}{3m\,\mathrm{Ca}_0}(\eta_{zz}+\eta_{zzzz})+\frac{M_0B}{2m(1+B)^2}\eta_{zz}-\frac{i}{2\pi m}\left(1-\frac{1}{m}\right)\int_{-\infty}^{\infty}N_K(k)\int_{-\infty}^{\infty}\eta(x,\tau)e^{ik(z-x)}dxdk=0. \tag{42}$$

Letting $x=zL$, $\nu=\left(1+\frac{3}{2}M_0\,\mathrm{Ca}_0\,B/(1+B)^2\right)^{-1}L^{-2}$, $\xi=6\,\mathrm{Ca}_0\,L^3\nu\eta$, $\beta=3\,\mathrm{Ca}_0/(2\pi)(1-1/m)\nu L^4$, and $T=1/(3m\,\mathrm{Ca}_0)\nu^{-1}L^{-4}\tau$, Eq. (42) reduces to the following canonical form:

$$\xi_T - \xi\xi_x + (\xi_{xx} + \nu\xi_{xxxx}) - i\beta\int_{-\infty}^{\infty} N_K(k)\int_{-\infty}^{\infty} \xi e^{ik(x-x')}dx'dk = 0. \quad (43)$$

This is a modified Kuramoto-Sivashinsky (KS) equation. It has already been established that the solution of KS equation remains bounded for general smooth initial conditions.[19–21] The dynamics of Eq. (43) have also been extensively studied previously.[7,22] The interfacial dynamics can either be chaotic or travelling motions, depending on ν and β. For sufficiently small ν and β, the evolution is chaotic. The effect of β is to introduce dispersion into the evolution, thus regularizing interfacial motion. Increasing $M_0B/(1+B)^2$ decreases both ν and β, suggesting that a cooler displacing fluid makes the system more susceptible to chaos.

VI. COMPARISON WITH PREVIOUS STUDIES

As shown above, our linear stability results for the isothermal case are identical to those of Georgiou *et al.*[5] For nonisothermal systems, our analysis can be compared with the study of Dijkstra and Steen.[16] In their analysis, the base flow is driven by an axial thermocapillary force. They showed that the instability can be suppressed by the shear stabilization arising from the basic flow. This shear effect is similar to that due to viscosity stratification in Eq. (37). In this regard, our results are in qualitative agreement with theirs albeit our basic flow differs from theirs.

Our work can also be relevant to flow inside the cylinder studied by Davalos-Orozco and You[17] (hereafter referred to as DY). DY demonstrated for flow inside the cylinder that the axisymmetric mode is generally the most unstable. Azimuthal modes can be excited but they are not as important as the axisymmetric mode. Inspecting our system using DY's results, we find that for parameters of our interest, the instability of our system is indeed dominated by the axisymmetric mode. Detailed findings of DY related to our work are described below.

DY showed for flow inside the cylinder that for all Ca/Pe (equivalent to their Cr) the most unstable mode is the axisymmetric mode for $\mathrm{Ma}<50$ although it coexists with azimuthal modes. In addition, as pointed out by DY, calculations of the maximum growth rate for a thin film also revealed that the axisymmetric mode is the most unstable.

Although most of DY's results are shown for the flow outside the cylinder, they may be applicable to our analysis if the fluid layer is sufficiently thin (i.e., large β in DY). As shown in their Fig. 4(b) for $\beta=10$ (corresponding to our $\varepsilon=0.1$), for $\mathrm{Cr}=\mathrm{Ca/Pe}=10^{-3}$ the maximum growth rate of the axisymmetric mode could be an order of magnitude larger than that of the first azimuthal mode for $\mathrm{Ma}<5$. In addition, the axisymmetric mode dominates for $\mathrm{Ma}<20$. Moreover, the smaller Cr, the more dominant the axisymmetric mode becomes, as shown in their Fig. 4(b) for $\mathrm{Cr}=10^{-6}$. In our study, since a typical Cr is $O(10^{-3})$ or smaller, and Ma $\sim O(1)$, the axisymmetric mode plays a more important role in determining instability than the azimuthal modes.

Physically speaking, when Cr is small, surface tension forces dominate and hence the capillary instability prevails. In this case, the axisymmetric mode usually dominates because the capillary instability is mainly triggered by the circumferential curvature $(1/r)$ that acts axisymmetrically. This is generally valid even when the annular thickness is not thin, as revealed in their Fig. 3(b) for $\beta=1$.

Furthermore, DY also found that for the same values of parameters, azimuthal modes excited for flow inside the cylinder are fewer than those for flow outside the cylinder. As such, the axisymmetric instability considered by the present study is adequate in view of its greater importance compared to azimuthal modes.

In qualitative aspects, our analysis can be compared with DY's axisymmetric-mode results for a thin film flow outside a cylinder. DY showed that the growth rates increase with Ma, indicating destabilizing effects due to thermocapillarity. In our work, similar results are also found analytically. In addition, concerning neutral stability, DY showed that thermocapillarity of $\mathrm{Ma}>0$ enlarges the unstable region in view of an increase in the critical wavenumber. A similar feature also can be obtained analytically in our study; it is demonstrated that to relieve the thermocapillary instability, shorter wavelengths are needed for enhancing the axial stabilization of capillarity.

It is worth noticing that although the axisymmetric mode is more important than the azimuthal modes in determining the linear instability of our system, it could take some time for the azimuthal modes to interact nonlinearly with the most unstable axisymmetric mode. Since that time scale could be the interval of validity for the nonlinear evolution equations found in the present analysis, the features of the subsequent nonlinear dynamics could differ from those predicted by the present axisymmetric study.

VII. APPLICATION OF THE PRESENT ANALYSIS

To validate the applicability of the present analysis, it is necessary to identify how physical properties vary with temperature. Typically, viscosity varies with temperature as $\mu \sim \exp(K/T)$, and hence its change due to the temperature variation is fairly small. For example, viscosity of air at 22 °C is $1.8\times\cdot 10^{-5}$ Pa s and that at 102 °C is 2.18×10^{-5} Pa s. This is only a 10% change for an 80 °C temperature difference. Viscosity of water at 20 °C is 10^{-3} Pa s. It reduces to 0.28×10^{-3} Pa s. at 100 °C. The average change is about 10^{-4} Pa s per 10 °C.

How density varies with temperature is reflected by the thermal expansion coefficient $\hat{\beta}=-1/\rho_0(\partial\rho/\partial T)_{T_0}$. Typical values of $\hat{\beta}$ range from 10^{-4} (for liquids) to 10^{-3} (for gases). Clearly, the temperature difference cannot be too large in our analysis, otherwise buoyancy would be significant. The significance of buoyancy can be estimated by the Grasshof number $\mathrm{Gr}=\hat{\beta}\Delta T^* g R_1^3/\nu^2$. For $\Delta T^*\sim 1$ °C and $R_1 \sim 10^{-2}$ cm, $\mathrm{Gr}=10^{-3}-10^{-4}$, and hence the effect can be neglected.

Although the change in interfacial tension due to the temperature variation is small (typically 0.1 dyn/cm °C), the induced thermocapillary forces could be comparable to viscous forces, depending on Ma. In our analysis, Ma could be $O(1)$.

In light of the above, effects of temperature on physical properties are generally not significant for temperature variations $<10\ ^\circ$C, and hence on Ca and Re.

As a typical example of a liquid-liquid displacement, consider an oil film of $\mu_2=10$ cP surrounding a water slug ($\mu_1=1$ cP) with an interfacial tension of 10 dyn/cm in a 200 μm diameter tube (whose circumference is 628 μm). The change in the interfacial tension due to the temperature variation is assumed to be 0.1 dyn/cm °C. A typical thermal conductivity of a common liquid is about 10^4 ergs/cm °C. Thermal diffusivity is on the order of 10^{-3} cm^2/s. A slug velocity can be as fast as 10 cm/s, and hence the estimated Peclet number is $O(10^2)$. The estimate of the heat transfer coefficient for such a slug is about 10^6 ergs/cm^2 °C. Consider a film thickness of 10 μm or $\varepsilon=0.1$. These numbers give $\mathrm{Re}_1\sim 10$, $\mathrm{Ca}\sim 10^{-2}$, $m=10$, and $B\sim 1$, which is in the range of validity of our analysis. With these parameters, the isothermal limit ($\mathrm{Ma}=0$) has a maximum growth rate of 0.05 min^{-1}, i.e., about a 14 min. doubling time, due to the capillary instability. The corresponding wavelength is 888 μm for $k_{\max}=1/\sqrt{2}\sim 0.71$ and the critical wave number is $k_c=1$. If the pore temperature is only slightly higher than water, say, 1 °C, this gives $\mathrm{Ma}\sim 1>0$ and the predicted maximum growth rate is 0.095 min^{-1}. This is almost twice the isothermal case. The corresponding wavelength is 757 μm ($k_{\max}\sim 0.83$), and the critical wavelength shifts to 443 μm ($k_c\sim 1.17$). On the other hand, for a cooler wall having the same temperature difference as the above, $\mathrm{Ma}\sim -1<0$ yields a maximum growth rate of 0.02 min^{-1}, that is a 60% reduction in the growth rate of the isothermal case. The corresponding wavelength is 1121 μm ($k_{\max}\sim 0.56$), and the critical wavelength shifts to 795 μm ($k_c\sim 0.79$). To completely suppress the capillary instability requires $\mathrm{Ma}\lesssim -8/3$. It means that the water temperature must be at least 2.3 °C lower than the wall temperature.

VIII. CONCLUDING REMARKS

We have studied the effects of thermocapillarity on the stability of a CAF in the thin-annulus limit ($\varepsilon\to 0$). Both linear and weakly nonlinear stabilities are examined. The analysis is carried out for two different sets of scalings: (i) $\mathrm{Ma}\sim O(1)$ and $\mathrm{Ca}\gtrsim\varepsilon^2$, and (ii) $\mathrm{Ma}\sim\varepsilon$ and $\mathrm{Ca}\gtrsim\varepsilon$. The first corresponds to the system with moderate thermocapillary and strong capillary forces; the second is in the regime of weak thermocapillary forces and moderately strong surface tension. The stability of case (i) is solely determined by the film flow, and that of case (ii) further includes the contribution from the core dynamics. Thermocapillarity in general linearly destabilizes (stabilizes) a CAF when the ambient core fluid is cooler (warmer) than the wall. It therefore encourages (discourages) the capillary instability.

The weakly nonlinear analysis shows that for case (i) the thermocapillary instability (due to a cooler core) could cause a large amplitude of the interface, so that it might be inclined to affect the integrity of a CAF. If the thermocapillary stabilization (due to a warmer core) is not sufficiently strong to completely suppress the capillary instability in the linear regime, the instability can be saturated within the weakly nonlinear regime, thereby keeping a CAF intact. As for case (ii), its weakly nonlinear dynamics are governed by the Kuramoto-Sivashinsky equation. Although the evolution remains bounded, thermocapillary effects could influence the route to chaos.

The implications of the present study to oil recovery processes are as follows. At the initial stages of the process, in order to efficiently displace crude oil lodged in porous media, it may be necessary for a displacing fluid to finger into capillaries without breaking into droplets. This requires an initially intact CAF configuration. A stabilizing effect on this CAF can be achieved by having a displacing fluid sufficiently hotter than the surrounding porous rocks. As the displacing fluid penetrates into the rocks, its temperature might become equal to that of the rocks, or might enter a region where the temperature of the rocks is higher than the fluid's. In this situation, thermocapillarity destabilizes. As a result, the displacing fluid might be in contact with the walls of the rocks or break up into droplets.

[1] L. Preziosi, K. Chen, and D. D. Joseph, "Lubricated pipelining: stability of core-annular flow," J. Fluid Mech. **201**, 323 (1989).
[2] T. R. Melli and L. E. Scriven, "Theory of 2-phase cocurrent downflow in networks of passages," Ind. Eng. Chem. Res. **30**, 951 (1991).
[3] J. C. Slattery, "Interfacial effects in the entrapment and displacement of residual oil," AIChE J. **20**, 1145 (1974).
[4] D. R. Otis, J. M. Johnson, T. J. Pedley, and R. D. & Kamm, "Role of pulmonary surfactant in airway closure: a computational study," J. Appl. Physiol. **75**, 1323 (1993).
[5] E. C. Georgiou, D. T. Papageorgiou, C. Maldarelli, and D. S. Rumschitzki, "An asymptotic theory for the linear stability of a core-annular flow in the thin annular limit," J. Fluid Mech. **243**, 653 (1992).
[6] A. L. Frenkel, A. J. Babchin, B. G. Levich, T. Shlang, and G. I. Sivashinsky, "Annular flows can keep unstable film from breakup: nonlinear saturation of capillary instability," J. Colloid Interface Sci. **115**, 225 (1987).
[7] D. T. Papageorgiou, C. Maldarelli, and D. S. Rumschitzki, "Nonlinear interfacial stability of core annular flows," Phys. Fluids A **2**, 340 (1990).
[8] V. Kerchman, "Strongly nonlinear interfacial dynamics in core-annular flows," J. Fluid Mech. **290**, 131 (1995).
[9] C. Kouris and J. Tsamopoulos, "Dynamics of axisymmetric core-annular flow in a straight tube. I. The more viscous fluid in the core, bamboo waves," Phys. Fluids **13**, 841 (2001).
[10] C. Kouris and J. Tsamopoulos, "Dynamics of the axisymmetric core-annular flow. II. The less viscous fluid in the core, saw tooth waves," Phys. Fluids **14**, 1011 (2002).
[11] J. R. A. Pearson, "On convection cells induced by surface tension," J. Fluid Mech. **4**, 489 (1958).
[12] L. E. Scriven and C. V. Sternling, "On cellular convection by surface-tension gradients: Effects of mean surface tension and surface viscosity," J. Fluid Mech. **19**, 321 (1964).
[13] D. A. Goussis and R. E. Kelly, "Surface wave and thermocapillary instabilities in a liquid film flow," J. Fluid Mech. **223**, 25 (1991).
[14] D. A. Goussis and R. E. Kelly, "On the thermocapillary instability in a liquid layer heated from below," Int. J. Heat Mass Transfer **33**, 2237 (1990).
[15] R. J. Deissler and A. Oron, "Stable localized patterns in thin liquid films," Phys. Rev. Lett. **68**, 2948 (1992).
[16] H. A. Dijkstra and P. H. Steen, "Thermocapillary stabilization of the capillary breakup of annular film of liquid," J. Fluid Mech. **229**, 205 (1991).
[17] L. A. Davalos-Orozco and X. You, "Three-dimensional instability of a liquid flowing down a heated vertical cylinder," Phys. Fluids **12**, 2198 (2000).
[18] M. K. Smith, "The long-wave instability in heated or cooled inclined liquid layers," J. Fluid Mech. **219**, 337 (1990).
[19] J. Goodman, "Stability of the Kuramoto-Sivanshinsky equation and related systems," Commun. Pure Appl. Math. **XLVII**, 293 (1994).

[20] J. S. II'yashenko, "Global analysis of the phase portrait for the Kuramoto-Sivanshinsky equation," J. Dyn. Differ. Equ. **4**, 585 (1992).
[21] P. Collet, J. P. Eckmann, H. Epstein, and J. Stubbe, "A global attracting set for the Kuramoto-Sivanshinsky equation," Commun. Math. Phys. **152**, 203 (1993).
[22] Y. S. Smyrlis and D. T. Papageorgiou, "Predicting chaos for infinite dimensional dynamical systems: The Kuramoto-Sivashinsky equation, a case study," Proc. Natl. Acad. Sci. U.S.A. **88**, 11129 (1991).